# Observer-based Adaptive Control for Slung Payload Stabilization with a Fully-actuated Multirotor UAV

Jorge Arizaga, Armando Miranda-Moya, Herman Castañeda, Pedro Castillo

# Observer-based Adaptive Control for Slung Payload Stabilization with a Fully-actuated Multirotor UAV

**Abstract**

This article presents an observer-based adaptive sliding mode controller for a fully-actuated hexacopter unmanned aerial vehicle, performing trajectory tracking in a perturbed environment while carrying a cable-suspended payload. Based on the unavailability of a payload swing sensor, an extended high-gain observer is designed, providing full-state and disturbance estimation including payload motion. Such disturbances are compensated into the control loop to dampen the oscillations, thus improving the flight performance of the hexacopter driven by the adaptive control, providing robustness against bounded perturbations and chattering reduction. The stability of the observer and the control method on this system is guaranteed through Lyapunov theory. Simulations using a multibody emulator demonstrate time reduction in payload dampening while controlling the aircraft trajectory, compared to a feedback regulation-based adaptive controller.

*Keywords:* **Hexacopter UAV, Cable Suspended Payload, Sliding Mode Control, Extended Observer.**

## 1. Introduction

In recent years, technological progress has had a significant relevance on the improvement of unmanned aerial vehicles (UAVs) capabilities, commonly deployed into environments that involve carrying out high-performance maneuvers, such as payload transportation for commercial services and disaster response [1, 2, 3], which has been implemented through the integration of robotic arms [4] or containers [5] on the body of the rotorcraft. Similarly, a different

approach relies on suspending the payload by attaching a cable directly to the UAV [6]. This method has been proposed to accomplish specific tasks like water collection and transportation for firefighting operations [7], and payload delivery in areas where the landing of the aircraft is extremely difficult [8]. However, the complexity of the system increases since the mechanism is susceptible to oscillations due to the lack of actuators to control the pendulum-like behavior of the suspended payload.

Strategies for cable swing attenuation have been previously addressed in the literature. Such as in [9] where an algorithm is proposed to establish the optimal trajectory between two points, reducing the oscillation of a payload hung to a quadcopter-type UAV (Quad-UAV). Additionally, the authors in [10] present a nonlinear backstepping controller that reduces the oscillations of a suspended payload attached to an underactuated hexacopter type UAV (UA-Hex) by rejecting the external disturbances that affect the vehicle due to wind using an open-loop and a feedback type trajectory generation approach. Nonetheless, these proposals usually require angle measurements of the payload swing, which could implicate the use of additional sensors or mechanisms.

To address the concerns related to the payload movement measurement, different approaches have been proposed. For instance, a passivity-based control scheme is presented in [11] and to reduce the oscillations of a suspended payload on a Quad-UAV, where the main advantage is that swing measurement is not required, as well as a robustification of this method for a Planar Vertical Take-off and Landing (PVTOL) vehicle with a suspended ball is described in [12]. Furthermore, in [13] a control based on an uncertainty and disturbance observer is proposed, where it is possible to maneuver the aircraft with a suspended load in a disturbed environment while reducing the oscillations. Similarly, in [14] a control scheme is given employing one perturbation observer together with an extended observer, to smooth out the payload dynamics on a Quad-UAV. In [15], the authors introduce an approach involving two nonlinear controllers. Their proposal exploits the coupling between the payload and the Quad-UAV position dynamics to mitigate the oscillations.

Prior studies employ underactuated multirotor UAVs (UA-UAVs), which, due to their aerodynamics, require coordinated control of their rotation and the thrust of their motors to displace the aircraft. This represents a disadvantage when it is necessary to reject environmental disturbances, especially when these disturbances are incident horizontally to the aircraft. As a result, new techniques have emerged to improve the flight performance of UAVs. Such is the case of [16] where a dynamic feature weight selection method for robust visual target tracking is proposed. Its authors report a superior performance of this method compared to others in the state-of-the-art.

To overcome these challenges, several alternatives have been proposed to convert UA-UAVs into fully-actuated devices [17] and expand their capabilities. One of the simplest modifications to enable a hexacopter UAV to exert horizontal forces is implementing a passive tilting of its motors, as reported in [18]. Inspired by this attribute, in [19] the authors presented a version of a fully actuated hexacopter, driven by an adaptive sliding mode controller (ASMC), performing a trajectory that does not require roll or pitch tilting. Additionally, the ASMC offers robustness against uncertainties and bounded perturbations, and reducing the stress on the actuators by regulating the control gains. Such action is directly related to the decrement of the chattering associated with conventional sliding modes.

Despite the availability of a considerable number of studies on UA-UAV payload transport, the research conducted with fully-actuated UAVs is limited. For this reason, in [20] has been proposed an oscillation reduction approach for a payload hanging on a fully-actuated hexacopter (FA-Hex). The study considers the unavailability of a hardware sensor to obtain the oscillation angles, therefore, an extended high-gain observer (EHGO) is proposed, which uses the hexacopter state measurements to estimate the payload motion. Since the dynamics of the payload are coupled to the displacement of the rotorcraft, the FA-Hex position control is driven by the combination of the EHGO and the ASMC (EHGO-ASMC), while the rotation control of the FA-Hex is operated with the feedback regulation-based ASMC scheme. Through this technique, it is possible to reduce

payload oscillations by estimating and compensating them in the control loop.

Therefore, the main contribution of the current manuscript relies on the improvement of the approach presented in [20], providing the closed-loop stability analysis of the observer-based control system by means of Lyapunov theory. Furthermore, the system previously described according to the Euler-Lagrange convention, is solved through the computer-assisted design (CAD) representation of our real hexacopter using SIMULINK/SIMSCAPE MULTIBODY software, which allows obtaining a closer representation of the dynamics of the experimental FA-Hex. Then, a reference trajectory is established for the FA-Hex to be performed in a disturbed environment. The same scenario is evaluated using two control approaches, in the first one, the EHGO-ASMC scheme is used, while in the second one, the feedback-regulation ASMC scheme is applied. The simulation comparison of these schemes, with a realistic trajectory scenario, evidences the feasibility of the EHGO-ASMC approach, by significantly reducing in magnitude and duration the payload oscillations produced by external disturbances and sudden changes of direction in the aircraft trajectory, with a proper management of the control effort as well as computing capacity requirement.

The paper is structured as follows: The dynamic model of the hexacopter-payload system is introduced in Section 2 , while the design of the EHGO-ASMC approach as well as the development of the closed-loop stability proof are given in Section 3. The simulations and the analysis of the results are shown in Section 4. Finally, the conclusions are summarized in Section 5.

## 2. System Dynamic Model

In this section, the model of the hexacopter-payload system is developed according to the Euler-Lagrange method. First, the reference frames are established and illustrated in Figure 1. The following payload conditions are considered: The cable has a constant known length and depreciated mass and deformation. The payload swing $\alpha_x$, $\alpha_y$ is limited to $-90° < \alpha_x < 90°$, and $-90° < \alpha_y < 90°$. The payload is represented as a constant weight ball, and

the air resistance is zero. Hence, this system is represented by:

$$\mathbf{M}(\mathbf{q})\ddot{\mathbf{q}} + \mathbf{C}(\mathbf{q}, \dot{\mathbf{q}})\dot{\mathbf{q}} + \mathbf{G}(\mathbf{q}) = \mathbf{u}, \tag{1}$$

where its elements are defined as follows:

- $\mathbf{q} = [\boldsymbol{\gamma},\ \boldsymbol{\eta},\ \boldsymbol{\mu_\alpha}]^T \in \mathbb{R}^8$, contains the generalized coordinates.
- $\boldsymbol{\gamma} = [x,\ y,\ z]^T \in \mathbb{R}^3$, expresses the hexacopter position.
- $\boldsymbol{\eta} = [\phi,\ \theta,\ \psi]^T \in \mathbb{R}^3$, denotes the hexacopter attitude.
- $\boldsymbol{\mu_\alpha} = [\alpha_x,\ \alpha_y]^T \in \mathbb{R}^2$, includes the cable swing angles.

From Figure 1, $\boldsymbol{\gamma_P} = [x_p, y_p, z_p]^T$ expresses the ball position. $L$ holds the wire length, whereas $l$ indicates the spacing from every propeller with respect to the aircraft center. The UAV and the payload weights are denoted by $M$ and $m$. By means of the Euler-Lagrange method, the Lagrangian $\mathcal{L}$ is determined:

$$\begin{aligned}
\mathcal{L} = {} & \frac{1}{2}(M+m)(\dot{x}^2 + \dot{y}^2 + \dot{z}^2) + \frac{1}{2}I_x\dot{\phi}^2 + \frac{1}{2}(I_yC_\phi^2 - I_zS_\phi^2)\dot{\theta}^2 \\
& + \frac{1}{2}(I_xS_\theta^2 + I_yC_\theta^2S_\phi^2 + I_zC_\phi^2C_\theta^2)\dot{\psi}^2 - I_xS_\theta\dot{\phi}\dot{\psi} + (I_y - I_z)C_\phi C_\theta S_\phi\dot{\theta}\dot{\psi} \\
& + \frac{1}{2}\left(mL^2C_{\alpha_y}^2 + I_p\right)\dot{\alpha_x}^2 + \frac{1}{2}\left(mL^2 + I_p\right)\dot{\alpha_y}^2 + mLC_{\alpha_x}C_{\alpha_y}\dot{\alpha_x}\dot{x} \\
& + mLS_{\alpha_x}C_{\alpha_y}\dot{\alpha_x}\dot{z} - mLS_{\alpha_x}S_{\alpha_y}\dot{\alpha_y}\dot{x} + mLC_{\alpha_y}\dot{\alpha_y}\dot{y} + mLC_{\alpha_x}S_{\alpha_y}\dot{\alpha_y}\dot{z} \\
& + Mgz + mg(z - LC_{\alpha_x}C_{\alpha_y}).
\end{aligned} \tag{2}$$

The matrices integrating the general system equation (1) are acquired by re-ordering the terms from (2). Therefore, the inertia matrix is:

$$\mathbf{M}(\mathbf{q}) = \begin{bmatrix} \mathbf{M_{MA}} & \mathbf{0}_{3\times3} & \mathbf{M_{CP}}^T \\ \mathbf{0}_{3\times3} & \mathbf{M_{PP}} & \mathbf{0}_{3\times2} \\ \mathbf{M_{CP}} & \mathbf{0}_{2\times3} & \mathbf{M_{CC}} \end{bmatrix} \in \mathbb{R}^{8\times8}, \tag{3}$$

with:

$$\mathbf{M_{MA}} = \begin{bmatrix} M_{11} & 0 & 0 \\ 0 & M_{22} & 0 \\ 0 & 0 & M_{33} \end{bmatrix};\ \mathbf{M_{PP}} = \begin{bmatrix} M_{44} & 0 & M_{46} \\ 0 & M_{55} & M_{56} \\ M_{64} & M_{65} & M_{66} \end{bmatrix};$$

$$\mathbf{M_{CP}} = \begin{bmatrix} M_{71} & 0 & M_{73} \\ M_{81} & M_{82} & M_{83} \end{bmatrix};\ \mathbf{M_{CC}} = \begin{bmatrix} M_{77} & 0 \\ 0 & M_{88} \end{bmatrix}.$$

Then, the Coriollis matrix is set as:

$$\mathbf{C}(\mathbf{q}) = \begin{bmatrix} \mathbf{0}_{3\times3} & \mathbf{0}_{3\times3} & \mathbf{C_{PP}} \\ \mathbf{0}_{3\times3} & \mathbf{C_{HR}} & \mathbf{0}_{3\times2} \\ \mathbf{0}_{2\times3} & \mathbf{0}_{2\times3} & \mathbf{C_{PR}} \end{bmatrix} \in \mathbb{R}^{8\times8}, \tag{4}$$

with

$$\mathbf{C_{HR}} = \begin{bmatrix} 0 & C_{45} & C_{46} \\ C_{54} & C_{55} & C_{56} \\ C_{64} & C_{65} & C_{66} \end{bmatrix}; \ \mathbf{C_{PP}} = \begin{bmatrix} C_{17} & C_{18} \\ 0 & C_{28} \\ C_{37} & C_{38} \end{bmatrix}; \ \mathbf{C_{PR}} = \begin{bmatrix} C_{77} & C_{78} \\ C_{87} & C_{00} \end{bmatrix}.$$

The gravity vector is:

$$\mathbf{G}(\mathbf{q}) = \begin{bmatrix} 0, & 0, & (m+M)g, & 0, & 0, & 0, & mLgS_{\alpha_x}C_{\alpha_y}, & mLgC_{\alpha_x}S_{\alpha_y} \end{bmatrix}^T, \tag{5}$$

and the system input is indicated by $\mathbf{u} = \mathbf{B}(\mathbf{q})\mathbf{F_M}$, where $\mathbf{B}(\mathbf{q}) \in \mathbb{R}^{8\times6}$ is a transformation matrix defined by

$$\mathbf{B}(\mathbf{q}) = \begin{bmatrix} \mathbf{B_{TP}}(\mathbf{q}) & \mathbf{0}_{3\times3} \\ \mathbf{0}_{3\times3} & \mathbf{B_{TA}}(\mathbf{q}) \\ \mathbf{0}_{2\times3} & \mathbf{0}_{2\times3} \end{bmatrix}, \tag{6}$$

with

$$\mathbf{B_{TP}}(\mathbf{q}) = \begin{bmatrix} B_{11} & B_{12} & B_{13} \\ B_{21} & B_{22} & B_{23} \\ B_{31} & B_{32} & B_{33} \end{bmatrix}; \ \mathbf{B_{TA}}(\mathbf{q}) = \begin{bmatrix} B_{44} & B_{45} & B_{46} \\ B_{54} & B_{55} & B_{56} \\ B_{64} & B_{65} & B_{66} \end{bmatrix}.$$

And $\mathbf{F_M} \in \mathbb{R}^6$ reflects the rotors forces generated over the FA-Hex frame. Hence: $\mathbf{F_M} = [\mathcal{F}_x, \mathcal{F}_y, \mathcal{F}_z, \tau_\phi, \tau_\theta, \tau_\psi]^T$. Such forces yield from the product between the allocation matrix $\mathbf{M}_\varphi$ and the vector $\mathbf{\Omega^2} \in \mathbb{R}^6$ which includes the square of the angular speed of all the motors. Then, $\mathbf{F_M} = \mathbf{M}_\varphi\mathbf{\Omega^2}$, and

$$\mathbf{M}_\varphi = \begin{pmatrix} M_{\varphi_{11}} & \cdots & M_{\varphi_{16}} \\ \vdots & \ddots & \vdots \\ M_{\varphi_{61}} & \cdots & M_{\varphi_{66}} \end{pmatrix} \in \mathbb{R}^{6\times6}. \tag{7}$$

The FA-Hex proposed is parameterized by the values given in TABLE I. The process to obtain the Lagrangian, as well as the values of the $\mathbf{M}(\mathbf{q})$, $\mathbf{C}(\mathbf{q})$, $\mathbf{B}(\mathbf{q})$, and $\mathbf{M}_\varphi$ matrices, are detailed in [19] and [20]. Through this model, it is possible to design the control scheme, which is developed in Section 3.

## 3. Controller Design

This section includes the observer-based controller design. Moreover, its stability proof using Lyapunov's theory is developed. In (1), the state vector $\mathbf{q}$ includes the payload swinging angles in terms of $\boldsymbol{\mu_\alpha}$. However, since this proposal assumes that such angle measurements are unavailable, Remark 1 is established. Then, the EHGO is proposed allowing the estimation of the position and velocity of the hexacopter, as well the external perturbations which include the payload swing. In addition, since the cable is hung exactly at the center of mass of the aircraft, the pendulum dynamics is matched only to the hexacopter position [10]. Therefore, the EHGO is designed for $\boldsymbol{\gamma} = [x,\ y,\ z]^T \in \mathbb{R}^3$.

**Remark 1.** *In the observer-based controller design, the effects of the payload are treated as perturbations, thus considering* $\mathbf{q} = [\boldsymbol{\gamma},\ \boldsymbol{\eta}]^T \in \mathbb{R}^6$.

The conventional sliding mode algorithm has some drawbacks, for instance the chattering issue, however, it offers significant advantages, such as robustness to bounded perturbations. Therefore, the adaptive term is included, which helps to minimize the chattering, preserving the robustness and convergence in finite time and reducing the excessive control effort. As a result, this approach consider a feedback regulation-based ASMC scheme for the attitude $\boldsymbol{\eta}$, while the FA-Hex position $\boldsymbol{\gamma}$ is operated by the EHGO-ASMC approach, as can be seen in the Figure 2.

To design the controller, let us take the system (1) assuming the Remark 1:

$$\begin{aligned} \dot{\mathbf{x}}_\mathbf{1} &= \mathbf{x_2}, \\ \dot{\mathbf{x}}_\mathbf{2} &= \mathbf{f}(\mathbf{x}, t) + \mathbf{g}(\mathbf{x})\mathbf{u} + \boldsymbol{d}(t), \\ \mathbf{y} &= \mathbf{x_1}, \end{aligned} \tag{8}$$

where $\mathbf{x_1} = \mathbf{q}$, $\mathbf{x_2} = \dot{\mathbf{q}}$, $\mathbf{f}(\mathbf{x}, t) = \mathbf{M}(\mathbf{q})^{-1}[-\mathbf{C}(\mathbf{q}, \dot{\mathbf{q}})\mathbf{q} - \mathbf{G}(\mathbf{q})]$, $\mathbf{g}(\mathbf{x}) = \mathbf{M}(\mathbf{q})^{-1}$, and $\mathbf{u} = \mathbf{B}(\mathbf{q})\mathbf{F_M}$. Load swing, as well as any externally disturbing forces, are considered in the term $\boldsymbol{d}(t)$. Therefore, the attitude controller is presented, and subsequently the EHGO-ASMC position control is designed.

### 3.1. ASMC attitude control

The control objective is to drive the position $\boldsymbol{e_\eta} = \boldsymbol{\eta} - \boldsymbol{\eta_d}$ and the angular velocity error $\dot{\boldsymbol{e}}_{\boldsymbol{\eta}} = \dot{\boldsymbol{\eta}} - \dot{\boldsymbol{\eta}}_{\boldsymbol{d}}$ to zero, for which the following sliding surface is established:

$$\boldsymbol{\sigma_a} = \dot{\boldsymbol{e}}_{\boldsymbol{\eta}} + \boldsymbol{\lambda}_{\boldsymbol{a}} \boldsymbol{e}_{\boldsymbol{\eta}}, \tag{9}$$

where, $\boldsymbol{\eta_d} \in \mathbb{R}^3$ indicates the attitude reference, while $\boldsymbol{\lambda_a} \in \mathbb{R}^{3\times3}$ is a diagonal matrix gain with $\lambda_{a,i} > 0$, for $i = 1, 2, 3$. Thus, the time derivative of $\boldsymbol{\sigma_a}$ is

$$\dot{\boldsymbol{\sigma}}_{\boldsymbol{a}} = (\mathbf{f}(\boldsymbol{\eta}, t) + \mathbf{g}(\boldsymbol{\eta})\mathbf{u_a}) - \ddot{\boldsymbol{\eta}}_{\boldsymbol{d}} + \boldsymbol{\lambda}_{\boldsymbol{a}} \dot{\boldsymbol{e}}_{\boldsymbol{\eta}}. \tag{10}$$

To fulfill the control objective, the following feedback control is proposed:

$$\mathbf{u_a} = \mathbf{g}(\boldsymbol{\eta})^{-1}(-\mathbf{f}(\boldsymbol{\eta}, t) - \boldsymbol{\lambda}_{\boldsymbol{a}} \dot{\boldsymbol{e}}_{\boldsymbol{\eta}} + \ddot{\boldsymbol{\eta}}_{\boldsymbol{d}} + \boldsymbol{\upsilon}_{\boldsymbol{aux_a}}), \tag{11}$$

where, $\boldsymbol{\upsilon}_{\boldsymbol{aux_a}} \in \mathbb{R}^3$ is the auxiliary term that includes the ASMC method:

$$\boldsymbol{\upsilon}_{\boldsymbol{aux_a}} = -\mathbf{K_a}(t) \left|\boldsymbol{\sigma_a}\right|^{1/2} \operatorname{sign}(\boldsymbol{\sigma_a}) - \mathbf{k_2}\boldsymbol{\sigma_a}, \tag{12}$$

with $\mathbf{k_2} \in \mathbb{R}^{3\times3}$ as a positive diagonal gain matrix, and $\mathbf{K_a(t)} \in \mathbb{R}^{3\times3}$ as a diagonal matrix of the adaptive gains, whose dynamics are described by

$$\dot{\mathbf{K}}_{\mathbf{a}}(\mathbf{t}) = \begin{cases} \mathbf{k_1} \operatorname{sign}(|\boldsymbol{\sigma_a}| - \boldsymbol{\mu_a}), & \text{if } \mathbf{K_a} > \mathbf{K_{min_a}}, \\ \mathbf{K_{min_a}}, & \text{if } \mathbf{K_a} \leq \mathbf{K_{min_a}}. \end{cases} \tag{13}$$

This scheme guarantees a minimum control effort with the diagonal matrix $\mathbf{K_{min_a}} \in \mathbb{R}^{3\times3}$, ensuring no zero control. Diagonal matrix gain $\mathbf{k_1} \in \mathbb{R}^{3\times3}$ adjusts the adaptation level, while $\boldsymbol{\mu_a} \in \mathbb{R}^3$ operates as the detection threshold for the sliding mode loss, triggering the increase or decrease of the control gains. It also provides the benefits of the standard sliding mode approach.

### 3.2. EHGO-ASMC position control

Consider the model from (8) taking into account only $\boldsymbol{\gamma}$, then: $\dot{\boldsymbol{\chi}}_{\mathbf{1}} = \boldsymbol{\chi}$, $\dot{\boldsymbol{\chi}}_{\mathbf{2}} = \mathbf{f}(\boldsymbol{\chi}, t) + \mathbf{g}(\boldsymbol{\chi})\mathbf{u_p} + \boldsymbol{\Delta}(t)$, $\mathbf{y} = \boldsymbol{\chi}_{\mathbf{1}}$, with, $\boldsymbol{\chi}_{\mathbf{1}} = \boldsymbol{\gamma}$, $\boldsymbol{\chi}_{\mathbf{2}} = \dot{\boldsymbol{\gamma}}$, and $\mathbf{f}(\boldsymbol{\chi}, t) = \mathbf{M}(\boldsymbol{\gamma})^{-1}[-\mathbf{C}(\boldsymbol{\gamma}, \dot{\boldsymbol{\gamma}})\dot{\boldsymbol{\gamma}} - \mathbf{G}(\boldsymbol{\gamma})]$, $\mathbf{g}(\boldsymbol{\chi}) = \mathbf{M}(\boldsymbol{\gamma})^{-1}$, and $\mathbf{u_p} = \mathbf{B}(\boldsymbol{\gamma})\mathbf{F_{x,y,z}}$. Vector

$\mathbf{u_p} = [u_x,\ u_y,\ u_z]^T$ expresses the position control input, while $\mathbf{F_{x,y,z}} \in \mathbb{R}^3$ the linear forces exerted by the motors. Hence, an extended third-order system is developed, which is valid only for the aircraft translation dynamics:

$$\begin{aligned} \dot{\chi}_{\mathbf{1}} &= \chi_{\mathbf{2}} \\ \dot{\chi}_{\mathbf{2}} &= \chi_{\mathbf{3}} + \hat{\mathbf{f}}(\hat{\chi}, t) + \hat{\mathbf{g}}(\hat{\chi})\mathbf{u_p} \\ \dot{\chi}_{\mathbf{3}} &= \xi(\chi) \\ \mathbf{y} &= \chi_{\mathbf{1}}. \end{aligned} \tag{14}$$

Perturbations are included in the state $\chi_{\mathbf{3}}$, such as the forces of the payload motion affecting the hexacopter:

$$\chi_{\mathbf{3}} = \mathbf{f}(\chi, t) - \hat{\mathbf{f}}(\hat{\chi}, t) + [\mathbf{g}(\chi) - \hat{\mathbf{g}}(\hat{\chi})]\mathbf{u_p}. \tag{15}$$

Thereby, the observer from [21] is chosen for the extended system (14), hence:

$$\begin{aligned} \dot{\hat{\chi}}_{\mathbf{1}} &= \hat{\chi}_{\mathbf{2}} + \frac{\kappa_{\mathbf{1}}}{\epsilon}(\chi_{\mathbf{1}} - \hat{\chi}_{\mathbf{1}}) \\ \dot{\hat{\chi}}_{\mathbf{2}} &= \hat{\chi}_{\mathbf{3}} + \hat{\mathbf{f}}(\hat{\chi}, t) + \hat{\mathbf{g}}(\hat{\chi})\mathbf{u_p} + \frac{\kappa_{\mathbf{2}}}{\epsilon^{\mathbf{2}}}(\chi_{\mathbf{1}} - \hat{\chi}_{\mathbf{1}}) \\ \dot{\hat{\chi}}_{\mathbf{3}} &= \frac{\kappa_{\mathbf{3}}}{\epsilon^{\mathbf{3}}}(\chi_{\mathbf{1}} - \hat{\chi}_{\mathbf{1}}), \end{aligned} \tag{16}$$

with $\boldsymbol{\epsilon}$ as the bandwidth gain, and factors $\boldsymbol{\kappa_{1,2,3}}$ are chosen as the polynomial $s^3 + \kappa_{\mathbf{1}} s^2 + \kappa_{\mathbf{2}} s + \kappa_{\mathbf{3}} = 0$ is Hurtwiz. This observer leads to the following ASMC design.

Similar to (9), the sliding surface is:

$$\boldsymbol{\sigma_p} = \dot{\hat{\boldsymbol{\gamma}}} - \dot{\boldsymbol{\gamma}}_{\boldsymbol{d}} + \boldsymbol{\lambda_p}(\hat{\boldsymbol{\gamma}} - \boldsymbol{\gamma_d}), \tag{17}$$

with $\boldsymbol{\gamma_d} \in \mathbb{R}^3$ as the reference position, and $\boldsymbol{\lambda_p} \in \mathbb{R}^{3\times 3}$ as a diagonal matrix gain with $\lambda_{p,i} > 0$, for $i = 1, 2, 3$. The time derivative of $\boldsymbol{\sigma_p}$ leads to,

$$\dot{\sigma}_{\mathbf{p}} = \left(\hat{\chi}_{\mathbf{3}} + \hat{\mathbf{f}}(\hat{\chi}, t) + \hat{\mathbf{g}}(\hat{\chi})\mathbf{u_p}\right) - \ddot{\gamma}_{\mathbf{d}} + \lambda_{\mathbf{p}}(\dot{\hat{\gamma}} - \dot{\gamma}_{\mathbf{d}}). \tag{18}$$

Finally, the following observer-based adaptive control is proposed:

$$\mathbf{u_p} = \hat{\mathbf{g}}(\hat{\boldsymbol{\chi}})^{-1}(-\hat{\boldsymbol{\chi}}_{\mathbf{3}} - \hat{\mathbf{f}}(\hat{\boldsymbol{\chi}}, t) - \boldsymbol{\lambda_p}(\dot{\hat{\boldsymbol{\gamma}}} - \dot{\boldsymbol{\gamma}}_{\boldsymbol{d}}) + \ddot{\boldsymbol{\gamma}}_{\boldsymbol{d}} + \boldsymbol{\upsilon_{paux}}), \tag{19}$$

where $\boldsymbol{\upsilon_{paux}}$ follows the ASMC described in (12) and (13), renaming the variables: $\boldsymbol{\upsilon_{aux_a}} \rightarrow \boldsymbol{\upsilon_{paux}}$, $\mathbf{K_a}(t) \rightarrow \mathbf{K_p}(t)$, $\sigma_{\mathbf{a}} \rightarrow \sigma_{\mathbf{p}}$, $\mathbf{k_2} \rightarrow \mathbf{k_4}$, $\mathbf{k_1} \rightarrow \mathbf{k_3}$,

$\boldsymbol{\mu_a} \rightarrow \boldsymbol{\mu_p}$, and $\mathbf{K_{min_a}} \rightarrow \mathbf{K_{min_p}}$. When $\hat{\boldsymbol{\gamma}}(0) \neq \boldsymbol{\gamma}(0)$, high-gain observers present a peaking phenomenon which leads the system to become unstable. To avoid such effects, control input $\mathbf{u_p}$ is passed through a saturation function as suggested in [22]. Then,

$$\mathbf{u_p} = \mathcal{W} \text{ sat } \left[ (\mathcal{W}\hat{\mathbf{g}}(\hat{\boldsymbol{\chi}})^{-1})(-\hat{\boldsymbol{\chi}}_{\mathbf{3}} - \hat{\mathbf{f}}(\hat{\boldsymbol{\chi}}, t) - \boldsymbol{\lambda_p}(\dot{\hat{\boldsymbol{\gamma}}} - \dot{\boldsymbol{\gamma}}_{\boldsymbol{d}}) + \ddot{\boldsymbol{\gamma}}_{\boldsymbol{d}} + \boldsymbol{\upsilon}_{\boldsymbol{paux}}) \right] \quad (20)$$

with, $\mathcal{W} > \max \left| \hat{\mathbf{g}}(\hat{\boldsymbol{\chi}})^{-1}(-\hat{\mathbf{f}}(\hat{\boldsymbol{\chi}}, t) - \boldsymbol{\lambda_p}(\dot{\hat{\boldsymbol{\gamma}}} - \dot{\boldsymbol{\gamma}}_{\boldsymbol{d}}) + \ddot{\boldsymbol{\gamma}}_{\boldsymbol{d}} + \boldsymbol{\upsilon}_{\boldsymbol{paux}}) \right|$, and $\text{sat}(a^*) = \min\{1, |a^*|\}\text{sign}(a^*)$.

The EHGO, estimates the full-state regarding the position of the FA-Hex as well as the disturbances that affect the vehicle, allowing then, its compensation, which results in a considerable oscillation reduction for the suspended payload.

### *3.3. EHGO-ASMC stability analysis*

The closed-loop stability analysis of the observer-based adaptive controller is addressed. Hence, the following definitions and lemmas are introduced.

#### *3.3.1. Definitions and lemmas*

Suppose a nonlinear system $h(x) : \mathbb{R}^n \rightarrow \mathbb{R}^n$ with $x \in \mathbb{R}^n$ such that

$$\dot{x} = h(x(t)), \quad x(t_0) = x_0, \quad h(0) = 0 \quad (21)$$

**Definition 1** [23]. The origin of (21) is finite-time stable if it is Lyapunov stable and any solution $x(t, t_0, x_0) = 0$, $\forall t \geq T_c(x_0) > 0$, with $T_c$ as the settling time.

**Definition 2** [24]. The solution of system (21) is practical finite-time stable if $\forall x(t_0) = x_0$ there is some $\digamma > 0$ and a settling time $T_c(\digamma, x_0) > 0$ that satisfy $||x(t)|| < \digamma \ \forall t \geq t_0 + T_c$.

**Lemma 1** [24, 25]. Suppose that a continuous function $V(x)$ exists for system (21) such that $V(0) = 0$ and $V(x) > 0$ for all $x \neq 0$. Therefore, the origin of (21) is practical finite-time stable if

$$\dot{V}(x) \leq c_1 V(x)^r + c_2 \quad (22)$$

with, $c_1, c_2 > 0$ and $0 < r < 1$. Furthermore, the trajectories of $x$ are bounded in finite-time as

$$\lim_{w \to w_0} x \in \left( V^r(x) \leq \frac{c_2}{(1-r)c_1} \right) \tag{23}$$

where, $0 < w \leq 1$, $0 < w_0 < 1$. Finally, the settling time function is given by

$$t_c \leq \frac{V^{1-r}(x_0)}{c_1 w_0 (1-r)} \tag{24}$$

*3.3.2. EHGO-ASMC convergence analysis*

Considering the fast dynamics of the observer, the term $(\frac{\kappa_i}{\epsilon^i})(\chi_1 - \hat{\chi}_1)$ for $i = 1, 2, 3$ from (16), converges to a region of small values $\omega(\epsilon)$ after a short period of time [26] since $(\chi_1 - \hat{\chi}_1) \to 0$. Therefore, the EHGO (31) can be analyzed as a follows

$$\dot{\hat{\chi}}_{\mathbf{1}} = \hat{\chi}_{\mathbf{2}} \tag{25}$$

$$\dot{\hat{\chi}}_{\mathbf{2}} = \hat{\mathbf{f}}(\hat{\chi}, t) + \hat{\mathbf{g}}(\hat{\chi})\mathbf{u_p} + \hat{\chi}_{\mathbf{3}} \tag{26}$$

where, the states vector $\boldsymbol{\chi} = [\hat{\chi}_1,\ \hat{\chi}_2,\ \hat{\chi}_3]^T$ describes the slow variables of the system, whilst the scaled estimation errors vector $\boldsymbol{\xi} = [\xi_1,\ \xi_2,\ \xi_3]^T$ with,

$$\xi_1 = \frac{\chi_1 - \hat{\chi}_1}{\epsilon^2},\ \ \xi_2 = \frac{\chi_2 - \hat{\chi}_2}{\epsilon},\ \text{and}\ \xi_3 = \chi_3 - \hat{\chi}_3 \tag{27}$$

represents the fast variables. Then, the following theorem is established:

**Theorem 1.** The observer-based control approach composed of the controller with practical finite-time convergence (19) and the EHGO with asymptotic convergence (16) forces the observation errors $(\chi_1 - \hat{\chi}_1)$, $(\chi_2 - \hat{\chi}_2)$, and $(\chi_3 - \hat{\chi}_3)$ to a region $\omega(\epsilon)$ with observer gain $\epsilon$ sufficiently small.

**Proof.** Recalling that $\chi_1 = \gamma_1$, $\chi_2 = \gamma_2$, and $\chi_3 = \gamma_3$, the observer-based controller (19) in closed loop with the dynamics (18) can be represented without loss of generality in single-input single-output form as:

$$u_p = \dot{\sigma}_p - \hat{\gamma}_3 \tag{28}$$

with,

$$\dot{\sigma}_p = -K_p(t)|\sigma_p|^{\frac{1}{2}}\text{sign}(\sigma_p) - k_4\sigma_p + \gamma_3 \tag{29}$$

Now, let [28]

$$V(\sigma_p) = \frac{1}{2}\sigma_p^2 + \frac{1}{2}(K_p(t) - K_s)^2 \tag{30}$$

be a Lyapunov candidate function for the stability analysis of the adaptive sliding mode scheme such that:

$$(K_p(t) - K_s) < 0 \tag{31}$$

$$K_s(t) > \frac{1}{|\sigma_p|^{\frac{1}{2}}}(Q_1 - k_4|\sigma_p|) \tag{32}$$

$$0 < |\gamma_3| \leq Q_1 \tag{33}$$

where $K_s$ refers to a certain value of the adaptive gain $K_p$ that guarantees the disturbance is counteracted, and $Q_1$ is the maximum bound of the disturbance term $\gamma_3$. Thus, as long as $K_p(t) > K_{min_p}$, the time differentiation of (30) is:

$$\dot{V}(\sigma_p) = \sigma_p\dot{\sigma_p} + (K_p(t) - K_s)(k_3 \text{ sign}(|\sigma_p| - \mu_p)) \tag{34}$$

Furthermore, by replacing (29) and (33) in (34), it yields:

$$\dot{V}(\sigma_p) \leq |\sigma_p|(-K_p(t)|\sigma_p|^{\frac{1}{2}}\text{sign}(\sigma_p) - k_4\sigma_p + Q_1) + (K_p(t) - K_s)(k_3 \text{ sign}(|\sigma_p| - \mu_p)) \tag{35}$$

Then, let terms $\pm K_s|\sigma_p|^{\frac{3}{2}}$ be included such that:

$$\dot{V}(\sigma_p) \leq |\sigma_p|(-K_s|\sigma_p|^{\frac{1}{2}} - k_4|\sigma_p| + Q_1) + (K_p(t) - K_s)(k_3 \text{ sign}(|\sigma_p| - \mu_p) - |\sigma_p|^{\frac{3}{2}}) \tag{36}$$

Now, consider the change of variable $\eta_p = K_s|\sigma_p|^{\frac{1}{2}} + k_4|\sigma_p| - Q_1$. Hence,

$$\dot{V}(\sigma_p) \leq -\eta_p|\sigma_p| + (K_p(t) - K_s)(k_3 \text{ sign}(|\sigma_p| - \mu_p) - |\sigma_p|^{\frac{3}{2}}) \tag{37}$$

Finally, let us aggregate $\pm\eta_q|K_p(t) - K_s|$ with, $\eta_p > 0$ and $|K_p(t) - K_s| = -(K_p(t) - K_s)$; to get:

$$\begin{aligned}
\dot{V}(\sigma_p) &\leq -\eta_p|\sigma_p| - \eta_q|K_p(t) - K_s| + |K_p(t) - K_s|(\eta_q - k_3 \text{ sign}(|\sigma_p| - \mu_p) + |\sigma_p|^{\frac{3}{2}}) \\
&\leq -\eta_p\frac{\sqrt{2}}{\sqrt{2}}|\sigma_p| - \eta_q\frac{\sqrt{2}}{\sqrt{2}}|K_p(t) - K_s| + |K_p(t) - K_s|(\eta_q - k_3 \text{ sign}(|\sigma_p| - \mu_p) + |\sigma_p|^{\frac{3}{2}}) \\
&\leq -\min\{\eta_p\sqrt{2}, \eta_q\sqrt{2}\}\Big(\frac{|\sigma_p|}{\sqrt{2}} + \frac{|K_p(t) - K_s|}{\sqrt{2}}\Big) \\
&+ |K_p(t) - K_s|(\eta_q - k_3 \text{ sign}(|\sigma_p| - \mu_p) + |\sigma_p|^{\frac{3}{2}})
\end{aligned} \tag{38}$$

Referring to Lemma 1, (38) can be rewritten in the form of a practical finite-time stable system

$$\dot{V}(\sigma_p) \leq -\eta_v V(\sigma_p)^{\varrho} + \chi_v \tag{39}$$

with $\eta_v = \min\{\eta_p\sqrt{2}, \eta_q\sqrt{2}\}$, $\varrho = 0.5$, and $\chi_v = |K_p(t) - K_s|[\eta_q - k_3 \text{ sign}(|\sigma_p| - \mu_p) + |\sigma_p|^{\frac{3}{2}}]$. Moreover, there is a value $\Gamma > 0$ and a finite-time $T_c(\Gamma, \sigma_{p_0})$ for all $\sigma_p$ that belongs to $\mathbb{R}$ such that $|\sigma_p| \leq \Gamma \ \forall t \geq t_0 + T_c$ [24]. Therefore, the achievement of the sliding mode can be divided in two phases: (1) the reaching phase when $|\sigma_p| > \Gamma$; and (2) the controller convergence when $|\sigma_p| \leq \Gamma$. Now, the following assumptions are taken into account:

**Assumption 1:** During the reaching phase of the sliding mode, all the trajectories from the sliding surface are bounded inside a positively invariant set:

$$\Xi_\zeta = \{V(\sigma_p) \leq \Upsilon_1\} \times \{|\sigma_p| \leq \zeta\} \tag{40}$$

Likewise, during the convergence phase, the trajectories of the sliding surface get inside a positively invariant set:

$$\Xi_\Gamma = \{V(\sigma_p) \leq \Upsilon_2\} \times \{|\sigma_p| \leq \Gamma\} \tag{41}$$

with boundary terms $\Upsilon_1 > \Upsilon_2$ and $\zeta > \Gamma \geq \mu_p$.

**Assumption 2:** The system error is bounded by $||e|| \leq h_1$ with $h_1 > 0 \ \forall t \geq t_0$. Furthermore, the system states are bounded by $||\gamma|| \leq h_1 + h_2$ with $h_2 > 0 \ \forall t \geq t_0$.

**Assumption 3:** There is a function $V_a(\gamma)$ that is bounded by class $\kappa$ functions $H_1$ and $H_2$ such that $H_1(||\gamma||) \leq V_a(\gamma) \leq H_2(||\gamma||) \ \ \forall \gamma \in D_\gamma$ with $D_\gamma$ as the domain of $\gamma$; and $\dot{V}_a < 0 \ \forall \|\gamma\| \geq \varphi(\|\gamma\|)$ with $\varphi$ as a continuous positive non-decreasing function.

**Assumption 4:** There is a boundary value $\varsigma \geq H_2(\varphi(||\gamma||))$ such that set $\{V_a(\gamma) \leq \varsigma\}$ is contained in the domain of all the solutions of the system.

According to [21], prior assumptions guarantee the boundedness of $\|\gamma\|$, and that sets $\rho_1 = \{V_a(\gamma) \leq \varsigma\} \times \Xi_\zeta$ and $\rho_2 = \rho_1 \times \Xi_\Gamma$ are positively invariant with respect to system (28). Hence, at time $t_1 \geq t_0$, $e$ enters $\rho_1$, and after a finite time $T_c > t_1$, $e$ enters $\rho_2$. Then, consider new terms:

$$\beta = \max_{\gamma \in \rho_2} \left| \frac{g(\gamma) - \hat{g}(\gamma)}{\hat{g}(\gamma)} \right| \tag{42}$$

$$W(s) = \frac{\kappa_3}{s^3 + \kappa_1 s^2 + \kappa_2 s + \kappa_3} \tag{43}$$

$$||W||_\infty = \sup_{Re(s)\geq 0} \mathcal{G}_{\max}(W(s)) \tag{44}$$

with, $||W||_\infty$ as the supremum maximum singular value ($\mathcal{G}_{\max}$) of transfer function $W(s)$ considering the right half plane [27]. It can be confirmed that $||W||_\infty = 1$ if all the poles of $W(s)$ are real. Now, suppose that [22]:

$$\beta < \frac{1}{||W||_\infty} \tag{45}$$

Furthermore, the scaled estimation error $\xi_3$ from (26) is rewritten as:

$$\xi_3 = f(\gamma) - \hat{f}(\gamma) + (g(\gamma) - \hat{g}(\gamma))u_p - \hat{\gamma}_3 \tag{46}$$

Since the saturation function from (20) is not continuously differentiable, a strategy from [29] is adopted. Thus, such function is replaced with the continuously differentiable term

$$\vartheta(q) = \begin{cases} q & \text{if } \ 0 \leq q \leq 1 \\ q + \frac{q-1}{\epsilon} - \frac{q^2-1}{2\epsilon} & \text{if } \ 1 < q < 1+\epsilon \\ 1 + \frac{\epsilon}{2} & \text{if } \ q \geq 1+\epsilon \end{cases} \tag{47}$$

which fulfills, $|\dot{\vartheta}(q)| \leq 1$ and whose results are close to the ones from the saturation function since $|\vartheta(q) - \text{sat}(q)| \leq \epsilon/2 \ \forall q \in \mathbb{R}$. Then, considering the time differentiation of vector $\boldsymbol{\xi}$, the closed-loop fast subsystem of the observer-based controller yields:

$$\epsilon\dot{\boldsymbol{\xi}} = \boldsymbol{\Lambda\xi} - \boldsymbol{\Psi_1}\left|\frac{g(\gamma) - \hat{g}(\gamma)}{\hat{g}(\gamma)}\right|\dot{\vartheta}\left(\frac{-\hat{\gamma}_3 - \hat{f}(\gamma) + \upsilon_{paux}}{M\hat{g}(\gamma)}\right)\kappa_3\xi_1 + \epsilon[\boldsymbol{\Psi_1}\Theta_1(\cdot) + \boldsymbol{\Psi_2}\Theta_2(\cdot)] \tag{48}$$

where, locally Lipschitz functions $\Theta_1$ and $\Theta_2$ are well defined in [26] and are bounded by $Q_b + Q_c\|\boldsymbol{\xi}\|$ with $Q_b, Q_c \in \mathbb{R}^+$; $\boldsymbol{\Psi_1} = [0,0,1]^T$, $\boldsymbol{\Psi_2} = [0,1,0]^T$, and matrix

$$\boldsymbol{\Lambda} = \begin{bmatrix} -\kappa_1 & 1 & 0 \\ -\kappa_2 & 0 & 1 \\ -\kappa_3 & 0 & 0 \end{bmatrix} \tag{49}$$

is Hurwitz. Furthermore, (48) holds if and only if $\gamma \in \rho_2$. Since $\epsilon[\mathbf{\Psi_1}\Theta_1(\cdot) + \mathbf{\Psi_2}\Theta_2(\cdot)]$ tends to a region $\omega(\epsilon)$ in a short period of time with sufficient small $\epsilon$, (48) can be reduced to:

$$\epsilon\dot{\boldsymbol{\xi}} = \mathbf{\Lambda\xi} - \mathbf{\Psi_1}\left|\frac{g(\gamma) - \hat{g}(\gamma)}{\hat{g}(\gamma)}\right|\dot{\vartheta}\left(\frac{-\hat{\gamma_3} - \hat{f}(\gamma) + \upsilon_{paux}}{M\hat{g}(\gamma)}\right)\kappa_3\xi_1 + \omega(\epsilon) \tag{50}$$

In the same way, it can be selected as a negative feedback for the transfer function

$$W(\epsilon s) = \frac{\kappa}{(\epsilon s)^3 + \kappa_1(\epsilon s)^2 + \kappa_2(\epsilon s) + \kappa_3} \tag{51}$$

Considering that $|\dot{\vartheta}(q)| \leq 1$, equation (45), and equality $\|W(\epsilon s)\|_\infty = \|W(s)\|_\infty$; the circle criterion analysis from [26] is followed to conclude that the origin of equation (50) is exponentially stable if and only if $\beta\|W(s)\|_\infty < 1$. Similarly, there is a Lyapunov candidate function $V_\xi(\boldsymbol{\xi}) = \boldsymbol{\xi}^T P_\xi \boldsymbol{\xi}$ bounded by $\epsilon^2 h_3$ with $h_3 > 0$ . Hence, for a sufficiently small $\epsilon$, a positive invariant set for the extended high-gain observer is defined as $\{V_\xi \leq \epsilon^2 h_3\}$. If the latter holds, set $\rho_{\text{obs}} = \rho_2 \times \{V_\xi \leq \epsilon^2 h_3\}$ is positive invariant as well. Then, as long as $(\boldsymbol{\gamma}, \boldsymbol{\xi})$ belongs to $\rho_{\text{obs}}$, $\xi_3 = \gamma(\epsilon)$ and [21]

$$u_p = \frac{-\hat{\gamma_3} - \hat{f}(\hat{x}) + \upsilon_{paux}}{\hat{g}(\hat{x})} = \frac{-f(x) + \upsilon_{paux}}{g(x)} + \omega(\epsilon) \tag{52}$$

Thus, with large enough saturation level and small enough bandwidth gain $\epsilon$ the output-feedback system can be written as:

$$\dot{\gamma}_1 = \gamma_2 + \omega(\epsilon) \tag{53}$$

$$\dot{\gamma}_2 = f(x) + g(x)u_p + \omega(\epsilon) \tag{54}$$

$$u_p = \dot{\sigma}_p + \omega(\epsilon) \tag{55}$$

$$\dot{\sigma}_p = -K_p|\sigma_p|^{\frac{1}{2}}\text{sign}(\sigma_p) - k_4\sigma_p \tag{56}$$

$$\epsilon\dot{\boldsymbol{\xi}} = \mathbf{\Lambda\xi} - \mathbf{\Psi_1}\left|\frac{g(x) - \hat{g}(x)}{\hat{g}(x)}\right|\dot{\vartheta}\left(\frac{-\hat{\gamma_3} - \hat{f}(x) + \upsilon_{paux}}{M\hat{g}(x)}\right)\kappa_3\xi_1 + \omega(\epsilon) \tag{57}$$

Scaled estimation error $\boldsymbol{\xi}$ achieves $\{V_\xi \leq \epsilon^2 h_3\}$ after a time $T_o \ll T_c$ since $T_o \to 0$ as $\epsilon \to 0$. Therefore, a proper small value of $\epsilon$ guarantees that the trajectories of $\boldsymbol{\gamma}$ get inside set $\rho_{\text{obs}}$ at a time $t_2 \geq T_o$; right after, they enter $\rho_2$ when $t_2 \geq T_c$. Thus, the proof is completed. □

## 4. Simulation Results

This section presents the numerical simulations of the performance comparison between the observer-based adaptive control approach versus the feedback regulation ASMC scheme in a perturbed environment. To get a closer system representation of the real FA-Hex platform, SolidWorks$^{TM}$ CAD and Simscape Multibody$^{TM}$ environment from MATLAB/Simulink$^{TM}$ are employed to assemble the prototype and model the system, respectively (see Figure 2).

The emulated flights consist in the tracking of a maze-shaped trajectory with a 50s duration, deployed on a 10m $\times$ 5m $\times$ 2m space. The FA-Hex is holding a ball of $m = 0.5$kg with a cable of $L = 1$m. The initial conditions for the system have been established as $\mathbf{q}(0) = [0, -1.5, 1.0, 0, 0, 0, 0, 0.43]^T$. The system is disturbed with a horizontal force incident on the FA-Hex defined by $P_x = 3$N, from $t = 29$s to $t = 37$s, representing a wind flow along the last section of the maze trajectory. The control and observer parameters are shown in TABLE II. Then, a Runge-Kutta solver with a 0.01s step is used.

Figure 3 shows both the FA-Hex and the payload trajectories driven by the ASMC and EHGO-ASMC schemes. In addition, the events of interest during the simulation are indicated. In both trajectories, payload oscillations caused by the initial condition and the disturbances are observed, however, the EHGO-ASMC scheme allows the FA-Hex to recover the reference trajectory while compensating and significantly reducing the pendulum motion. Otherwise, the ASMC gives a lower performance, since oscillation prevails after the disturbance forces.

The evolution of the oscillations from the payload for both controllers is displayed in Figure 4. At $t = 14s$, an oscillation occurs in the $\alpha_x$ angle for both scenarios, which is caused by the aircraft trajectory change. Under the EHGO-ASMC scheme, the vehicle is able to attenuate such swinging within $7s$, unlike the ASMC case, where the oscillation still exists at the time another perturbation appears at $t = 21s$. Here, this oscillation is being dampened by the EHGO-ASMC, until the wind disturbance happens at $t = 29s$. Subsequent to this perturbation, the EHGO-ASMC again attenuates the oscillation and it

does it in 5s, while with the ASMC this remain up to the end of the trajectory. The plot of $\alpha_y$ shows the effect of the payload initial condition, as well as that of the hexacopter direction changes, and the perturbation at $t = 29s$. For the above three situations, the EHGO-ASMC effectiveness in smoothing oscillations is demonstrated. In addition, the time evolution of the payload coordinates with $x_p$, $y_p$, and $z_p$ is shown. Considering the $x_p$ vs $y_p$ data, the superiority of the proposed observer-based controller scheme is noticeable.

Figure 5 displays the aircraft position and attitude driven by both control schemes. The capability of the UAV to travel using lateral forces, while the attitude is stabilized can be observed. Additionally, the effects of the initial condition and the perturbation at $t = 29s$ are highlighted to show that the EHGO-ASMC scheme compensates for the pendulum motion of the payload by making temporary deviations of the trajectory. Figure 6 shows that the forces and torques required for tracking and external disturbances rejection, as well as compensate for the swinging, remain within the capabilities of the actual hexacopter. Furthermore, this suggests a robust behavior of the controller, without requiring excessive stress on the actuators.

Regarding the EHGO, the performance is detailed in Figure 7(a), where the estimation error $\hat{e}_\gamma = \gamma - \hat{\gamma}$ remains below 0.01m for the three observed axes. Figure 7(b) shows the perturbations $\chi_3$ affecting the FA-Hex on its $x$ and $y$ axes, as well as their estimations $\hat{\chi}_3$. In addition, TABLE III shows the performance index for both scenarios. Since the payload motion is compensated with the horizontal displacement of the UAV, the ASMC scheme shows slightly better performance for FA-Hex trajectory tracking, but with continuous oscillation of the payload. These results indicate that the observer-based adaptive control scheme EHGO-ASMC is particularly suitable for the oscillation damping of a payload carried by a fully-actuated hexacopter, providing an appropriate control effort management, despite the external disturbances. Finally, the use of any additional device to measure the payload dynamics is obviated.

## 5. Conclusions

In this research, an observer-based adaptive sliding mode controller has been developed for a fully actuated hexacopter unmanned aerial vehicle subject to disturbances while carrying a payload suspended by cable during a trajectory tracking task. Considering the nonexistence of a device to measure the payload motion, an extended high gain observer has been proposed, allowing to estimate the complete aircraft state, as well as external disturbances, including those caused by the payload. These estimations have been compensated in the control loop, to reduce the cable oscillations and improve the flight performance. Moreover, the proposal has been analyzed using the Lyapunov theory, guaranteeing stability. Then, to demonstrate the performance and robustness of this strategy, a perturbed simulated scenario has been set up in Simscape Multibody$^{\mathrm{TM}}$ environment from MATLAB/Simulink$^{\mathrm{TM}}$. The results of this scheme have been compared with those using an adaptive controller which does not compensate for the estimation of the payload motion inside the control loop. Simulation results demonstrate that the observer-based adaptive control approach provides superior abilities to a fully-actuated hexacopter to attenuate the oscillations of a suspended payload while developing a predefined trajectory.

## Acknowledgments

This research was partially supported by the CONACyT and Tecnologico de Monterrey, in collaboration with the UTC Heudiasyc Lab.

[1] Ruggiero F, Lippiello V, Ollero A. Aerial Manipulation: A Literature Review. IEEE Robot Autom Lett 2018;3:1957–64. https://doi.org/10.1109/LRA.2018.2808541.

[2] Villa DKD, Brandão AS, Sarcinelli-Filho M. Load Transportation Using Quadrotors: A Survey of Experimental Results. 2018 Int. Conf. Unmanned Aircr. Syst., 2018, p. 84–93. https://doi.org/10.1109/ICUAS.2018.8453296.

[3] Villa DKD, Brandão AS, Sarcinelli-Filho M. A Survey on Load Transportation Using Multirotor UAVs. J Intell Robot Syst 2020;98:267–96. https://doi.org/10.1007/s10846-019-01088-w.

[4] Ballesteros-Escamilla MF, Cruz-Ortiz D, Chairez I, Luviano-Juárez A. Adaptive output control of a mobile manipulator hanging from a quadcopter unmanned vehicle. ISA Trans 2019;94:200–17. https://doi.org/10.1016/j.isatra.2019.04.002.

[5] Schneider D. The delivery drones are coming. IEEE Spectr 2020;57:28–9. https://doi.org/10.1109/MSPEC.2020.8946304.

[6] Wu Y, Xie Y, Li S. Parameter Adaptive Control for a Quadrotor With a Suspended Unknown Payload Under External Disturbance. IEEE Access 2021;9:139958–67. https://doi.org/10.1109/ACCESS.2021.3119396.

[7] Qin H, Cui JQ, Li J, Bi Y, Lan M, Shan M, et al. Design and implementation of an unmanned aerial vehicle for autonomous firefighting missions. 2016 12th IEEE Int. Conf. Control Autom., 2016, p. 62–7. https://doi.org/10.1109/ICCA.2016.7505253.

[8] Xia K, Lee S, Son H. Adaptive control for multi-rotor UAVs autonomous ship landing with mission planning. Aerosp Sci Technol 2020;96:105549. https://doi.org/https://doi.org/10.1016/j.ast.2019.105549.

[9] Hashemi D, Heidari H. Trajectory Planning of Quadrotor UAV with Maximum Payload and Minimum Oscillation of Suspended Load Using Optimal Control. J Intell Robot Syst 2020;100:1369–81. https://doi.org/10.1007/s10846-020-01166-4.

[10] Klausen K, Fossen TI, Johansen TA. Nonlinear Control with Swing Damping of a Multirotor UAV with Suspended Load. J Intell Robot Syst 2017;88:379–94. https://doi.org/10.1007/s10846-017-0509-6.

[11] Guerrero-Sánchez ME, Mercado-Ravell DA, Lozano R, García-Beltrán CD. Swing-attenuation for a quadrotor transporting a cable-suspended payload. ISA Trans 2017;68:433–49. https://doi.org/10.1016/j.isatra.2017.01.027.

[12] Guerrero-Sánchez ME, Hernández-González O, Valencia-Palomo G, Mercado-Ravell DA, López-Estrada FR, Hoyo-Montaño JA. Robust IDA-PBC for underactuated systems with inertia matrix dependent of the unactuated coordinates: application to a UAV carrying a load. Nonlinear Dyn 2021;105:3225–38. https://doi.org/10.1007/s11071-021-06776-7.

[13] Qian L, Liu HHT. Path-Following Control of A Quadrotor UAV With A Cable-Suspended Payload Under Wind Disturbances. IEEE Trans Ind Electron 2020;67:2021–9. https://doi.org/10.1109/TIE.2019.2905811.

[14] Guo K, Jia J, Yu X, Guo L, Xie L. Multiple observers based anti-disturbance control for a quadrotor UAV against payload and wind disturbances. Control Eng Pract 2020;102:104560. https://doi.org/10.1016/j.conengprac.2020.104560.

[15] Guerrero-Sánchez ME, Lozano R, Castillo P, Hernández-González O, García-Beltrán CD, Valencia-Palomo G. Nonlinear control strategies for a UAV carrying a load with swing attenuation. Appl Math Model 2021;91:709–22. https://doi.org/10.1016/j.apm.2020.09.027.

[16] An Z, Wang X, Li B, Xiang Z, Zhang B. Robust visual tracking for UAVs with dynamic feature weight selection. Appl. Intell 2022. https://doi.org/10.1007/s10489-022-03719-6.

[17] Rashad R, Goerres J, Aarts R, Engelen JBC, Stramigioli S. Fully Actuated Multirotor UAVs: A Literature Review. IEEE Robot Autom Mag 2020;27:97–107. https://doi.org/10.1109/MRA.2019.2955964.

[18] Jiang G, Voyles RM. Dexterous UAVs for Precision Low-Altitude Flight. In: Valavanis KP, Vachtsevanos GJ, editors. Handb. Unmanned Aer. Veh., Dordrecht: Springer Netherlands; 2015, p. 207–37. https://doi.org/10.1007/978-90-481-9707-1_130.

[19] Arizaga JM, Castañeda H, Castillo P. Adaptive Control for a Tilted-Motors Hexacopter UAS Flying on a Perturbed Environment. 2019 Int. Conf. Unmanned Aircr. Syst., 2019, p. 171–7. https://doi.org/10.1109/ICUAS.2019.8798048.

[20] Arizaga JM, Castañeda H, Castillo P. Payload Swing Attenuation of a Fully-Actuated Hexacopter via Extended High Gain Observer Based Adaptive Sliding Control. 2021 Int. Conf. Unmanned Aircr. Syst., 2021, p. 901–8. https://doi.org/10.1109/ICUAS51884.2021.9476819.

[21] Khalil HK. High-gain observers in nonlinear feedback control. SIAM; 2017. https://doi.org/10.1137/1.9781611974867.

[22] Khalil HK. Extended High-Gain Observers as Disturbance Estimators. SICE J Control Meas Syst Integr 2017;10:125–34. https://doi.org/10.9746/jcmsi.10.125.

[23] Polyakov A, Fridman L. Stability notions and Lyapunov functions for sliding mode control systems. J Franklin Inst 2014;351:1831–65. https://doi.org/10.1016/j.jfranklin.2014.01.002.

[24] Zhu Z, Xia Y, Fu M. Attitude stabilization of rigid spacecraft with finite-time convergence. Int J Robust Nonlinear Control 2011;21:686–702. https://doi.org/10.1002/rnc.1624.

[25] Wang F. Adaptive finite-time control for a class of uncertain high-order nonlinear systems based on fuzzy approximation. IET Control Theory Appl 2017;11:677-684(7). https://doi.org/10.1049/iet-cta.2016.0947.

[26] Freidovich LB, Khalil HK. Performance Recovery of Feedback-Linearization-Based Designs. IEEE Trans Automat Contr 2008;53:2324–34. https://doi.org/10.1109/TAC.2008.2006821.

[27] Bruinsma, N. A., & Steinbuch, M. A fast algorithm to compute the $H_\infty$-norm of a transfer function matrix. Syst. Control. Lett. 1990; 14(4), 287-293. https://doi.org/10.1016/0167-6911(90)90049-Z

[28] Plestan F, Shtessel Y, Brégeault V, Poznyak A. New methodologies for adaptive sliding mode control. Int J Control 2010;83:1907–19. https://doi.org/10.1080/00207179.2010.501385.

[29] Nazrulla S, Khalil HK. Robust Stabilization of Non-Minimum Phase Nonlinear Systems Using Extended High-Gain Observers. IEEE Trans Automat Contr 2011;56:802–13. https://doi.org/10.1109/TAC.2010.2069612.

TABLE I. Parameters of the FA-Hex.

| **Parameter** | **Value** | **Unit** | **Parameter** | **Value** | **Unit** |
|---|---|---|---|---|---|
| $M$ | 1.71 | kg | $I_p$ | 0.0013 | $(\text{kgm}^2)$ |
| $l$ | 0.23 | m | $\varphi$ | 20 | deg |
| $g$ | 9.81 | $\text{m/s}^2$ | $\alpha_1$ | 30 | deg |
| $I_x$ | 0.0266 | $(\text{kgm}^2)$ | $\alpha_2$ | $-30$ | deg |
| $I_y$ | 0.0268 | $(\text{kgm}^2)$ | $\alpha_3$ | $-90$ | deg |
| $I_z$ | 0.0434 | $(\text{kgm}^2)$ | $\alpha_4$ | $-150$ | deg |
| $m$ | 0.50 | kg | $\alpha_5$ | 150 | deg |
| $L$ | 1.0 | m | $\alpha_6$ | 90 | deg |

TABLE II. Controller and observer parameters.

| **Attitude** | | **EHGO** | | **Position** | |
|---|---|---|---|---|---|
| *Parameter* | *Value* | *Parameter* | *Value* | *Parameter* | *Value* |
| $\lambda_{\phi,\theta,\psi}$ | diag(1.2, 1.2, 2.5) | $\kappa_{\mathbf{1_{x,y,z}}}$ | $[3.0;\ 3.0;\ 1.0]^T$ | $\lambda_{x,y,z}$ | diag(1.5, 1.5, 3.0) |
| $k_{1_{\phi,\theta,\psi}}$ | diag(0.5, 0.5, 0.5) | $\kappa_{\mathbf{2_{x,y,z}}}$ | $[3.0;\ 3.0;\ 1.0]^T$ | $k_{3_{x,y,z}}$ | diag(1.0, 1.0, 1.5) |
| $k_{min_{\phi,\theta,\psi}}$ | diag(0.01, 0.01, 0.1) | $\kappa_{\mathbf{3_{x,y,z}}}$ | $[3.0;\ 3.0;\ 1.0]^T$ | $k_{min_{x,y,z}}$ | diag(0.1, 0.1, 0.1) |
| $\mu_{\phi,\theta,\psi}$ | diag(0.2, 0.2, 0.2) | $\epsilon$ | 0.10 | $\mu_{x,y,z}$ | diag(0.1, 0.1, 0.1) |
| $k_{2_{\phi,\theta,\psi}}$ | diag(2.5, 2.5, 7.5) | | | $k_{4_{x,y,z}}$ | diag(3.0; 3.0; 10) |

TABLE III. Performance index of the simulated results.

| | **MSE** | | **ITAE** | | $\|\|u\|\|_2$ | |
|---|---|---|---|---|---|---|
| | *EHGO-ASMC* | *ASMC* | *EHGO-ASMC* | *ASMC* | *EHGO-ASMC* | *ASMC* |
| $X$ | 0.1408 | 0.1922 | 230.36 | 378.94 | 40.520 | 51.617 |
| $Y$ | 0.0606 | 0.0568 | 130.59 | 123.23 | 126.74 | 125.11 |
| $Z$ | 0.0019 | 0.0019 | 49.799 | 49.606 | 2189.1 | 2190.0 |
| $\phi$ | 0.0155 | 0.0153 | 95.601 | 98.172 | 14.807 | 15.628 |
| $\theta$ | 0.0004 | 0.0009 | 15.235 | 24.015 | 5.7270 | 7.2758 |
| $\psi$ | 0.1009 | 0.1000 | 135.11 | 134.45 | 4.9489 | 4.9710 |
| $\alpha_x$ | 0.0042 | 0.0166 | 41.550 | 124.41 | | |
| $\alpha_y$ | 0.0063 | 0.0146 | 56.194 | 89.579 | | |

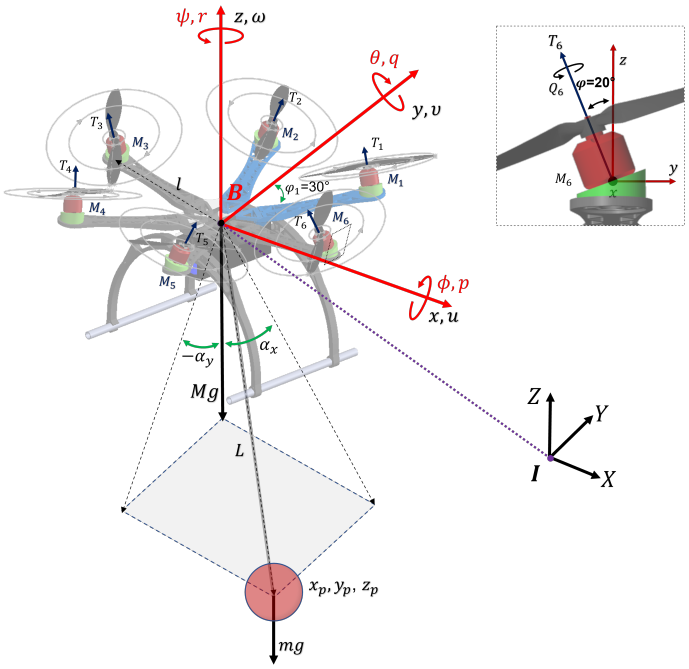


Figure 1. Reference frames of the fully-actuated hexacopter UAV together with the suspended payload.

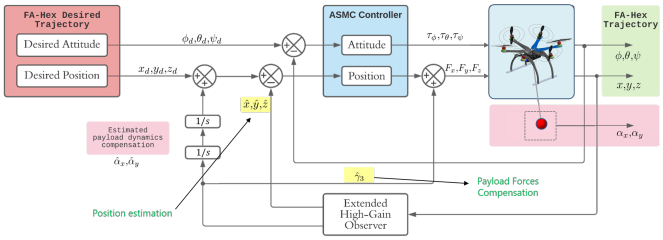


Figure 2. Observer-based adaptive EHGO-ASMC diagram for the FA-Hex trajectory with payload swing reduction. The system model has been solved with Simscape Multibody$^{TM}$ environment from MATLAB/Simulink$^{TM}$

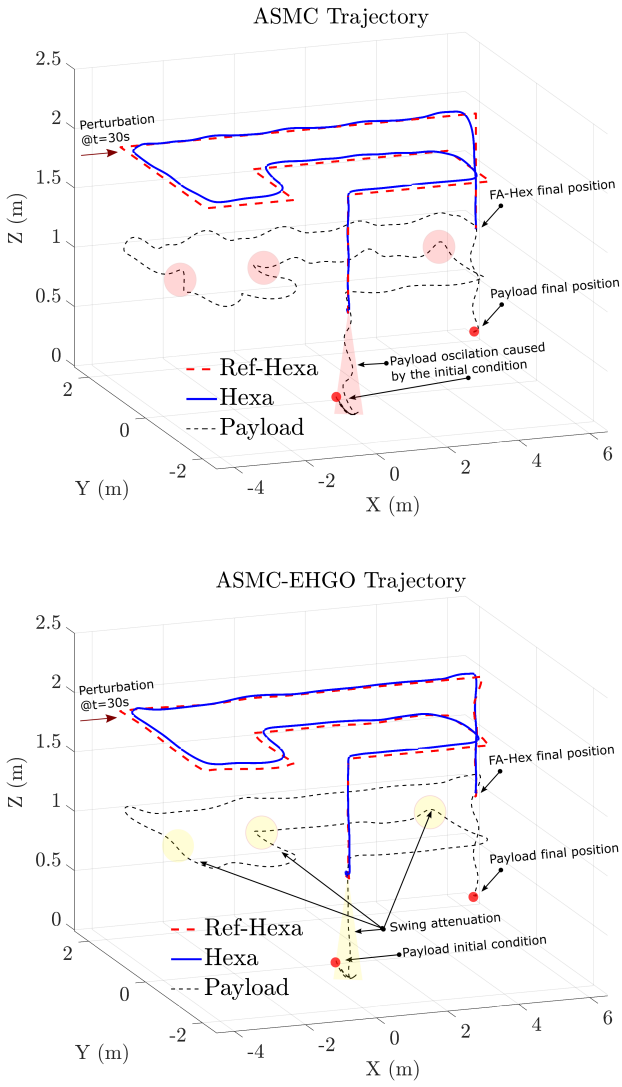


Figure 3. A three-dimensional representation of the trajectory followed by the hexacopter and the payload. Events of interest in both simulations are highlighted.

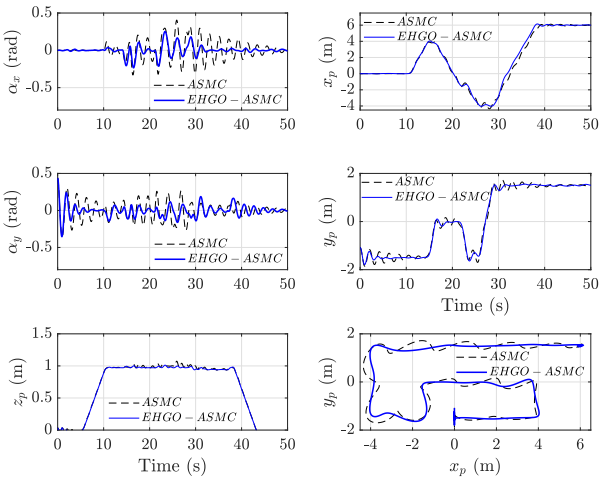


Figure 4. Payload dynamics along the simulation. The superiority of the adaptive observer-based controller to reduce the oscillations faster and in the presence of disturbances is observed.

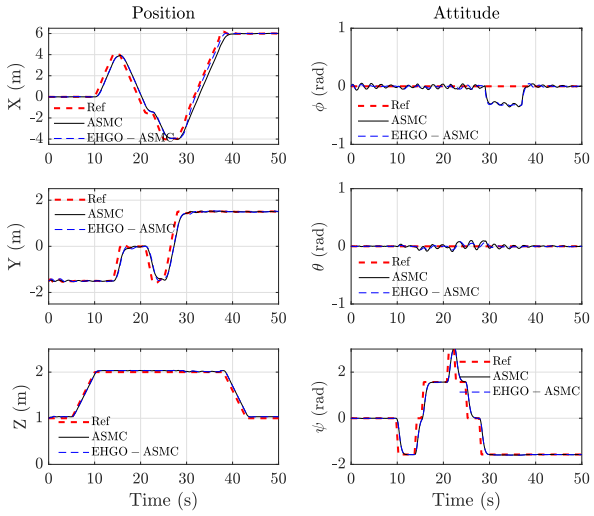


Figure 5. UAV flight trajectories. Small deviations required by the FA-Hex for the oscillations reduction are observed.

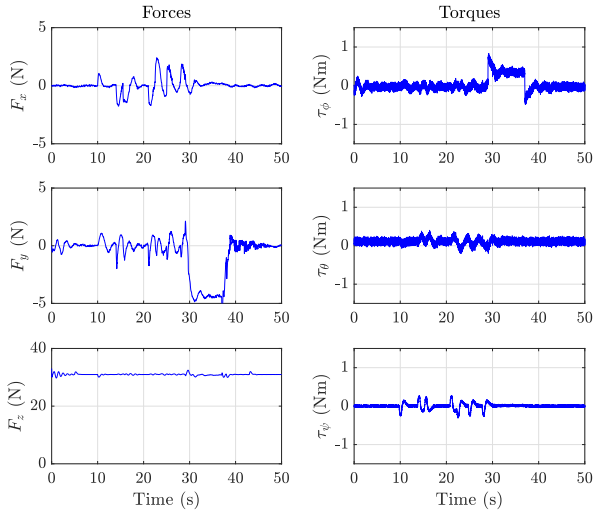


Figure 6. Forces required by the UAV driven by the EHGO-ASMC. The action of the horizontal forces for the rejection of oscillations and trajectory tracking is shown.

[Hexacopter estimation errors by EHGO.]

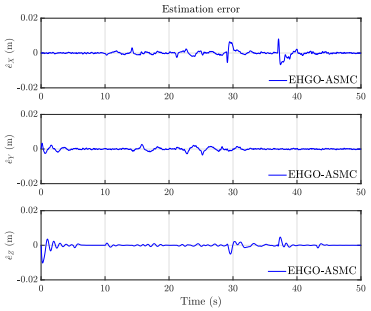


[Payload and perturbations estimation.]

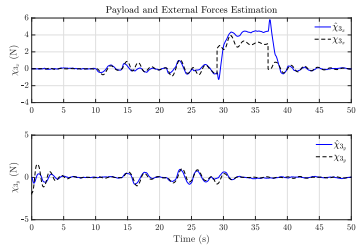


Figure 7. Observer performance on the estimation of the hexacopter position, as well as payload motion and external perturbations.